

# Noninvasive MRI of tissue redox state based on endogenous chemical exchange saturation transfer (CEST) contrast

Kejia Cai<sup>1,2</sup>, He N Xu<sup>1</sup>, Anup Singh<sup>1</sup>, Lily Moon<sup>1</sup>, Mohammad Haris<sup>1,3</sup>, Xiaohong Joe Zhou<sup>2</sup>, Ravinder Reddy<sup>1</sup>, and Lin Z Li<sup>1</sup>

<sup>1</sup>Radiology, University of Pennsylvania, Philadelphia, PA, United States, <sup>2</sup>CMRR 3T Research Program, Radiology, University of Illinois at Chicago, Chicago, IL, United States, <sup>3</sup>Sidra Medical and Research Center, Doha, Qatar

**Target audience:** Research scientists or clinicians who are interested in cancer metabolism, oxidative stress and redox state.

**Introduction/Purpose:** Cellular redox state has been demonstrated as a key player in cellular biology. The disturbed balance of the redox state, such as excessive oxidative stress, can lead to many pathologic changes including cancer, heart diseases, neurodegenerative diseases, and diabetes. Imaging biomarkers for oxidative stress are a key research area<sup>1-3</sup>. Tumor redox state heterogeneity revealed by the optical redox scanning of *ex vivo* tissues may differentiate tumor aggressiveness<sup>4</sup>. However, the redox scanning is highly invasive, limiting its use. The purpose of this study is to develop a non-invasive MR imaging method for mapping the tissue redox state based on the endogenous Chemical Exchange Saturation Transfer (CEST) contrast. We report herein a CEST MRI technique, together with correlations to the optical redox scanning to characterize tumor redox heterogeneity. The mechanism on such correlation has also been investigated.

**Methods:** All animal experiments on two human breast cancer mouse xenograft models, MDA-MB-231 (n=8) and MCF-7 (n=6), were performed according to an Institutional Animal Care and Use Committee approved protocol. The tumors were grown as previously described<sup>5</sup> and the tumor volumes ranged from 100 mm<sup>3</sup> to 1000 mm<sup>3</sup>. CEST Z-spectra images of the tumor central slice with saturation offsets from -5 to 5 ppm and a step-size of 0.25 ppm were collected on a 9.4T Varian small animal MR scanner using a customized sequence<sup>6</sup>, which consists of a frequency selective rectangular saturation pulse (B<sub>1</sub>=250 Hz, 1 s) followed by a segmented Fast Low-Angle SHot (FLASH) readout. Both B<sub>0</sub> and B<sub>1</sub> field inhomogeneity maps were acquired for the correction of CEST contrast maps from +2 to +4 ppm, normalized to the corresponding negative saturation offsets as previously reported<sup>6</sup>. In addition, magnetization transfer (MT) images, T<sub>1</sub>- and T<sub>2</sub>-weighted images of the same slice were also acquired. After MRI, the tumor-bearing mice under anesthesia underwent snap-freezing procedures and the excised frozen tumors were embedded for multi-slice fluorescence imaging of NADH (reduced form of nicotinamide adenine dinucleotide) and Fp (oxidized flavoproteins) using the Chance redox scanner to quantify the NADH redox ratio, NADH/(Fp+NADH)<sup>5</sup>. We then performed CEST MRI of the solutions of the major metabolites (see Figure 3) in two redox reactions, representative of many others *in vivo* in a general form of  $RH_2 + NAD^+ \leftrightarrow R + NADH + H^+$ , where R is the substrate. As NAD<sup>+</sup> and NADH concentrations are <1 mM *in vivo* and the additional proton (H) in NADH is associated with a carbon, their difference in CEST contrast is negligible. All solutions were freshly prepared in PBS at pH 7.0 and maintained at 37 °C.

**Results:** The multi-modality MRI study (Figure 1A-D) demonstrates that only CEST MRI showed distinctive core-rim patterns from the MDA-MB-231 tumors (rim to core ratio 1.54 ± 0.17) comparing to the MCF-7 tumors (1.21 ± 0.19, p<0.05). This rim to core separation appeared independent of the CEST saturation offset from +2 to +4 ppm (Figure 1E). CEST contrasts from individual tumor rim and core are linearly correlated with the NADH redox ratios quantified by the optical redox scanning (p=0.00002, Figure 2). Through the phantom studies on the metabolites in two representative redox reactions (Figure 3), we found that the reductants (in this case, glutamate and alanine) generally expressed a higher CEST contrast than the corresponding oxidants (oxoglutarate and pyruvate) due to the reception of mobile protons through the NAD(P)/NAD(P)H mediated redox reactions. This explains why higher tissue CEST contrast *in vivo* corresponded to more reduced redox state as shown in Figure 2B.

**Discussion:** Our study demonstrates that CEST MRI is capable of revealing the tumor rim to core bimodal pattern, as observed by the optical redox scanning. The quantitative and significant correlation between the CEST MRI and the optical scanning indicates that the overall CEST contrast *in vivo* can be an imaging biomarker of the NADH redox ratio. This correlation is supported by the phantom studies on the metabolites of two redox reactions which are representative of many other redox reactions *in vivo*. Non-invasive CEST MRI of tissue redox state, as a new imaging marker, may find new clinical applications in diagnosis of cancer as well as other diseases. It is worth noting that the overall CEST contrast *in vivo* may also be affected by other factors, including tissue pH, T<sub>1</sub> and T<sub>2</sub>, and the metabolites that are not involved in redox reactions. Hence, CEST MRI of tissue redox state requires calibration and the comparison may only be made between similar tissue types. Despite these limitations, this study demonstrates a novel MRI technique sensitive to tissue redox state.

**References:** [1].Cook JA, et al. Oxidative stress, redox, and the tumor microenvironment. *Seminars in Radiation Oncology*. 2004;14:259-66. [2].Barnham KJ, et al. *Nat Rev Drug Discov*. 2004;3:205-14. [3].Allen RG, et al. *Free Radic Biol Med*. 2000;28:463-99. [4].Li LZ, et al. *PNAS*. 2009;106:6608-13. [5]. Xu HN, et al. *Journal of biomedical optics*. 2010;15:036010. [6].Cai K, et al. *Nat Med*. 2012;18:302-6.

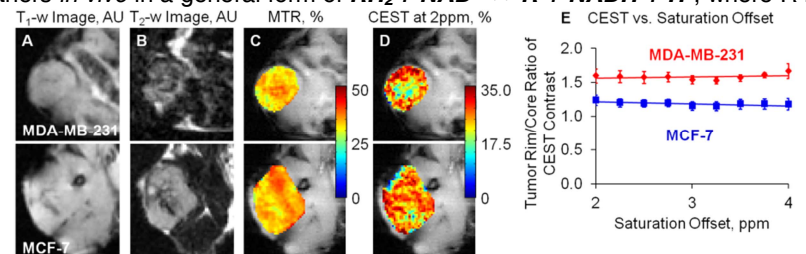


**Figure 1.** Images of the two breast cancer models: MDA-MB-231 (top) and MCF-7 (bottom) with multi-modality MRI: T<sub>1</sub>-weighted (T<sub>1</sub>-w, A), T<sub>2</sub>-weighted (T<sub>2</sub>-w, B), magnetization transfer ratio (MTR) (C) and CEST at 2ppm (D). T<sub>1</sub>, T<sub>2</sub>-weighted and MTR contrast does not exhibit a clear bimodal rim to core pattern in either of the tumor models. Only the CEST contrast exhibits clear rim to core separation from the MDA-MB-231 tumor. (E) Relationships between saturation offset and the rim-to-core ratio of the CEST contrast for the two breast cancer animal models.

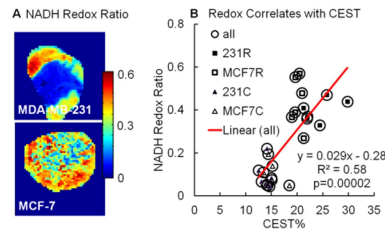


**Figure 2.** (A) NADH redox ratio maps obtained from the optical redox scanning of representative MDA-MB-231 (top) and MCF-7 (bottom) tumors. (B) Significant correlation between NADH redox ratio and CEST contrast is illustrated from individual tumor cores (C) and rims (R) (p=0.00002).

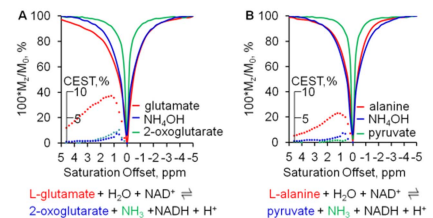


**Figure 3.** Z spectra (solid lines) and the rescaled CEST asymmetrical curves (dots) of the key metabolites in two representative redox reactions. A) 10 mM glutamate (red), 34 to 125 mM NH<sub>4</sub>OH (blue), 50 mM 2-oxoglutarate (green). B) 10 mM alanine (red), 34 to 125 mM NH<sub>4</sub>OH (blue), 10 mM pyruvate (green).